Catalysis Science & Technology

ROYAL SOCIETY OF CHEMISTRY

REVIEW

View Article Online
View Journal | View Issue

Cite this: *Catal. Sci. Technol.*, 2026, **16**, 1902

Modulated excitation DRIFTS and steady-state isotopic transient kinetic analysis (SSITKA) of NH_3-SCR-DeNO$_x$ on Cu-containing zeolite Y

Magdalena Jabłońska,*[ab] Rujito S. R. Suharbiansah,[ac] Jie Yang,[d] Marek Rotko,[e] Pranjit Das,[f] Marko Bertmer,[f] Jacek Grams,[g] Junjiang Zhu[d] and Andreas Pöppl[f]

As-received commercial zeolite Y (in the forms of Na^+, H^+, and NH_4^+) with an *n*(Si)/*n*(Al) ratio of about 2.6 modified with copper cations was investigated in the selective catalytic reduction of nitrogen oxide with ammonia (NH_3-SCR-DeNO$_x$). Operando diffuse reflectance infrared Fourier transform spectroscopy (DRIFT) experiments using concentration modulation excitation (ME) coupled with phase-sensitive detection (PSD) analysis, together with steady-state isotopic transient kinetic analysis (SSITKA), were carried out to study key transient adsorbates on Cu-containing zeolite Y samples. We could observe different interactions between NO exposure to the NH_3 preadsorbed surface over the applied catalysts. For CuY_CBV100, NO exposure to an NH_3-preadsorbed surface leads to a decrease in NH_3 bound to Lewis acid sites (L-NH_3) and the formation of new Brønsted acid sites (B-NH_3). Part of the L-NH_3 migrates to these newly generated BAS. Based on the modulation excitation results, we could set the order of activity of the applied catalysts. For CuY_CBV500, the situation differs. A strong B-NH_3 peak indicates a high concentration of Brønsted acid sites on the CuY_CBV500 surface. NO can react with both L-NH_3 and B-NH_3, and the presence of B-NH_3 contributes to the high N_2 selectivity observed. SSITKA revealed that CuY_CBV100 exhibited a higher number of active centers on its surface, thus leading to higher NO conversion during NH_3-SCR-DeNO$_x$, but its reactivity is slightly lower than in the case of the other studied materials (especially CuY_CBV500).

Received 15th December 2025,
Accepted 21st January 2026

DOI: 10.1039/d5cy01536g

rsc.li/catalysis

1. Introduction

The selective catalytic reduction of NO with ammonia (NH_3-SCR-DeNO$_x$; 4 NH_3 + 4NO + O_2 → 4 N_2 + 6 H_2O) is an effective way of treating nitrogen oxide emissions to meet increasingly stringent international emission standards (*e.g.*, ref. 1 and 2). The ability of Cu-containing zeolites to convert NO into N_2 in the presence of ammonia over Cu–Y was first discovered in Japan in 1977. In this study, Seiyama *et al.*[3] already proposed a Langmuir–Hinshelwood type of reaction of NO and NH_3 coordinated to Cu(II) ions. According to the Langmuir–Hinshelwood (L–H) mechanism, the SCR reaction process occurs *via* adsorbed NH_3 species and adsorbed NO_x^- species. Otherwise, in the Eley–Rideal (E–R) mechanism, the reaction occurs between adsorbed ammonia species (NH_x; $x < 3$) on redox sites and NO from the gas phase.[1,4,5] Furthermore, NH_3-SCR-DeNO$_x$ over Cu-containing zeolites was approved to follow redox mechanisms, consisting of a reduction half-cycle and oxidation half-cycle. The reaction mechanism was investigated *via* numerous spectroscopic methods, such as *in situ* DR UV-vis or *in situ* FT-IR (*e.g.*, ref. 6–8). Otherwise, transient techniques such as modulated excitation DRIFTS or steady-state isotopic transient kinetic analysis (SSITKA) are less frequently investigated. Operando diffuse reflectance infrared Fourier transform spectroscopy (DRIFTS) experiments using concentration modulation excitation (ME) coupled with phase sensitive detection (PSD) analysis have been demonstrated to detect dynamic species that are directly involved in catalytic reactions (*e.g.*, ref. 9–12). Vibrational signals of reactive species can be obtained by combining ME with *in situ* infrared (IR) spectroscopy. This approach

[a] *Institute of Chemical Technology, Universität Leipzig, Linnéstr. 3, Leipzig 04103, Germany. E-mail: magdalena.jablonska@chemia.uni.lodz.pl*
[b] *University of Łódź, Faculty of Chemistry, Department of Inorganic and Analytical Chemistry, Tamka 12, Łódź 91-403, Poland*
[c] *Department of Sustainable Fuels and Green Chemistry, University of Chemistry and Technology, Technická 5, 166 28 Prague 6, Czech Republic*
[d] *Hubei Key Laboratory of Biomass Fibers and Eco-dyeing and Finishing, College of Chemistry and Chemical Engineering, Wuhan Textile University, Wuhan 430200, China*
[e] *Department of Chemical Technology, Institute of Chemical Sciences, Faculty of Chemistry, Maria Curie-Sklodowska University, Maria Curie-Sklodowska Sq. 3, Lublin, 20-031, Poland*
[f] *Felix Bloch Institute for Solid State Physics, Universität Leipzig, Linnéstr. 5, Leipzig 04103, Germany*
[g] *Institute of General and Ecological Chemistry, Faculty of Chemistry, Lodz University of Technology, Zeromskiego 116, Lodz, 90-924, Poland*

effectively removes the signals from unreactive species that do not vary at the same frequency as the ME on, isolating only the dynamic components relevant to the reaction. Through phase-sensitive detection (PSD) analysis, time-resolved spectra are transformed into phase-resolved spectra that capture signals exclusively from species responding to the modulation sequence. As a result, signals from unresponsive or static species are effectively removed, while those from active and perturbed species are highlighted. Modulation excitation diffuse reflectance infrared Fourier transform spectroscopy (ME DRIFTS) has previously been employed to investigate the reaction mechanisms of NH_3-SCR-DeNO$_x$ over V_2O_5/TiO_2 and V_2O_5/WO_3-TiO_2,[13,14] Cu-SSZ-13,[15] as well as CeO_2 and WO_3/CeO_2.[9]

SSITKA, developed largely through the work of Biloen,[16] Bennett,[17] Happel,[18] and Bell,[19] is a technique used in heterogeneous catalysis to gain insight into the reaction pathways of surface-catalyzed processes. The SSITKA method is a widely recognized technique that allows for the determination of key kinetic parameters under actual reaction conditions. SSITKA provides information on the homogeneity or heterogeneity of the catalyst surface, offering valuable insight into possible reaction mechanisms. The simplest approach involves analyzing the shape of the curves that depict changes in product concentration over time following a switch between reactants with different isotopic compositions.[20] SSITKA was already applied to study the reaction mechanism over zeolites Cu–Y (ref. 21) and Cu-SSZ-13,[7,22] and revealed kinetic parameters, such as average-surface lifetime, surface concentration and intrinsic activity over the applied catalysts.

Both SSITKA and modulated studies offered direct spectroscopic evidence of key transient intermediates and their kinetic parameters. Thus, in the present study, a series of commercially available zeolite Y samples were modified with copper cations, fully characterized in terms of their physicochemical properties, and further evaluated for the NH_3-SCR-DeNO$_x$ activity and N_2 selectivity. The reaction mechanism was evaluated *via* steady-state isotopic transient kinetic analysis (SSITKA), and modulated studies were supported *via* temperature-programmed methods. Thus, this work is a continuation of our previous work[21] on commercial zeolite Y applied in NH_3-SCR-DeNO$_x$. However, in the present study, our approach was dictated by economic considerations, *i.e.*, commercially available zeolites in various forms (Na^+, NH_4^+, and H^+) were used without any other modification.

2. Experimental

2.1. Catalyst preparation

Table 1 shows the commercially available zeolite Y samples purchased from Zeolyst that were applied in this study. As-received samples (*i.e.*, without any pretreatment) were ion-exchanged using a 0.05 M aqueous solution of copper(II) acetate (≥98 wt%, Alfa Aesar) at room temperature (*ca.* 25 °C) for 24 h (1 g of zeolite per 100 ml of copper precursor solution). Finally, the samples were filtered and thoroughly washed until pH 7 was reached, dried, and calcined at 550 °C for 4 h in static air (with a heating rate of 1 °C min^{-1}).

Table 1 The data for commercially available zeolites used in this study were provided by the manufacturer. The *n*(Si)/*n*(Al) ratios are as specified by the manufacturer[23]

Sample	Form	*n*(Si)/*n*(Al)	Treatment[24]
CBV100	Na^+	2.55	Parent zeolite
CBV300	NH_4^+	2.55	Ion-exchanged
CBV400	H^+	2.55	Ion-exchanged
CBV500	NH_4^+	2.6	Ion-exchanged, mildly steamed

2.2. Catalyst characterization and catalytic experiments

The zeolite Y samples and their Cu-containing forms (CuY) were characterized using X-ray diffraction (XRD), N_2 sorption, scanning electron microscopy analysis (SEM), time-of-flight secondary ion mass spectrometry (ToF-SIMS), solid-state nuclear magnetic resonance (NMR), inductively coupled plasma optical emission spectroscopy (ICP-OES), diffuse reflectance UV-vis spectroscopy (DR UV-vis), and temperature-programmed reduction (TPR-H_2). All Cu-containing Y samples were examined for their catalytic activity and N_2 selectivity in NH_3-SCR-DeNO$_x$. The reaction mechanism was thoroughly evaluated *via* transient techniques (steady-state transient isotopic analysis, SSITKA) and modulated excitation DRIFTS, supported *via* temperature-programmed studies. The details of the experimental procedure can be found in the SI.

3. Results and discussion

3.1. Structural and textural/redox properties

Fig. 1a and S1a show the XRD patterns of the pristine Y and Cu-modified zeolite Y. The ion exchange process did not alter the primary peaks in the XRD pattern of the Y-type zeolite. Fig. 1b and S1b–d present the N_2 adsorption–desorption isotherms measured at −196 °C. According to the IUPAC classification,[25] all samples possess mixed type I and type IV characteristics with a dominant micropore volume (Table S1). The textural properties of the pristine zeolite Y samples decrease after modification with copper, indicating partial blockage of the zeolite pores. The copper content varied in the range of 3.8–8.3 wt% along with an *n*(Cu)/*n*(Al) ratio of 0.17–0.42 (Table 2).

The morphology of the copper-containing CuY_CBV300 sample is shown in Fig. 1c, while the SEM micrographs of the remaining Cu-containing zeolite Y samples are presented in Fig. S2. All materials exhibited the typical morphology of faujasite-type zeolites, consisting of agglomerated cubic crystals with well-defined edges and smooth surfaces.[26] The particles displayed relatively uniform shapes without any noticeable structural collapse or fragmentation after copper ion exchange and subsequent calcination at 550 °C. Interestingly, although the CuY_CBV300 sample showed

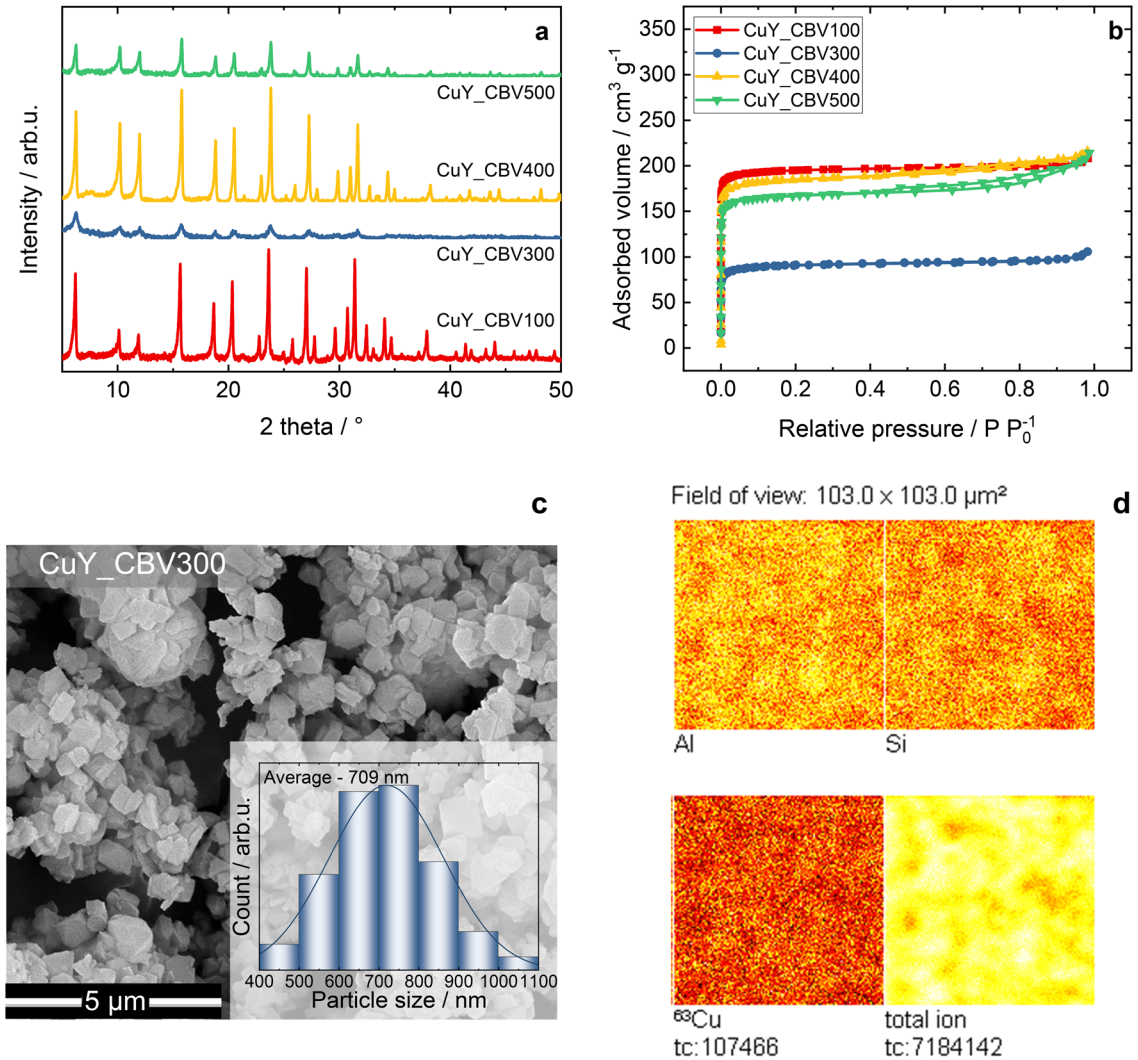

Fig. 1 a) XRD patterns and b) N_2 sorption isotherms of the Cu-containing zeolite Y samples and c) SEM images of CuY_CBV300. The particle size distribution was obtained by measuring 100 particles from SEM images and d) ToF-SIMS images collected from the surface of CuY_CBV300 (tc - total counts).

Table 2 Elemental composition (ω_i: mass fractions), n(Si)/n(Al) and n(Cu)/n(Al) ratios of the calcined zeolite Y samples and their Cu-containing forms

Sample	ω_{Al}/wt%	ω_{Si}/wt%	ω_{Na}/wt%	ω_{Cu}/wt%	n(Si)/n(Al)	n(Cu)/n(Al)
CBV100	9.9	25.7	8.9	—	2.49	—
CuY_CBV100	8.3	28.2	2.6	8.2	3.26	0.42
CBV300	11.1	28.2	1.9	—	2.45	—
CuY_CBV300	9.9	29.2	0.4	6.1	2.87	0.26
CBV400	11.3	28.0	1.9	—	2.38	—
CuY_CBV400	8.8	27.6	0.2	4.8	3.01	0.23
CBV500	10.8	30.0	0.1	—	2.67	—
CuY_CBV500	8.8	30.1	0.1	3.6	3.29	0.17

more distinct changes in its textural properties according to N_2 sorption analysis (*e.g.*, specific surface area and pore volume), the SEM images did not reveal any pronounced morphological differences compared to the other CuY_CBV samples. The average particle size distributions, determined using ImageJ software, were in the range of 678–851 nm. This slight increase in size can be attributed to the partial aggregation of crystallites during the copper ion-exchange and calcination steps. Overall, SEM analysis confirms that copper introduction did not alter the primary morphology of the zeolite Y crystals, and the structural properties of the faujasite framework were well preserved.

Fig. 1d, S3 and S4 show the spatial distribution of selected ions (Al^+, Si^+, Cu^+, and total ion$^+$) on the surfaces

of the analyzed samples, collected over areas of approximately 100 × 100 μm, while Tables S2 and S3 summarize the intensity ratios of selected ions calculated from the acquired spectra. The obtained results indicate that the distribution of the analyzed ions on the surface of the tested materials is generally homogeneous, and the morphology of their surface is rather responsible for certain inhomogeneities observed in the images. On the other hand, notable variations in the intensity of signals originating from the main components of the analyzed samples were noted. The lowest values of the Al^+/Si^+ intensity ratio were found for CBV300 and CuY_CBV300 (0.75 and 1.14, respectively), suggesting the lowest aluminum concentrations. For the remaining samples, the Al^+/Si^+ intensity ratio varied between 2.99 and 4.69 for zeolites, and 1.31 and 3.51 for Cu-containing materials. A different trend was observed for the Cu^+/Al^+ intensity ratio, which reached its highest value for the CuY_CBV100 sample (0.66). This catalyst also exhibited the highest value of Cu^+/total ion^+ (0.019). In contrast, variations in the Cu^+/Si^+ ratio were less pronounced, ranging from 0.62 for CuY_CVB300 to 0.93 in the case of CuY_CVB400.

Fig. 2a shows the DR UV-vis spectra of Cu-containing zeolite Y samples (calcined at 550 °C for 4 h in static air). For all samples, well-defined and distinct peaks were observed. According to the literature, the absorption bands in the 200–260 nm range can be attributed to oxygen-to-metal charge-transfer transitions associated with Cu^+ or Cu^{2+} cations stabilized within the zeolite framework.[27,28] The bands observed between 260 and 550 nm indicate the presence of Cu_xO_y species and $[Cu–O–Cu]^{2+}$ species.[29,30] However, in our previous study,[21] we excluded the presence of $[Cu–O–Cu]^{2+}$ species in the Cu-containing zeolite Y samples. Absorption in the 550–900 nm region is assigned to the d–d transitions of Cu^{2+} ions in pseudo-octahedral coordination, such as $Cu(H_2O)_6^{2+}$.[27,28] Fig. 2b and S5 show the solid-state ^{29}Si and ^{27}Al NMR spectra of the Cu-containing zeolite Y samples, while Tables S4 and S5 present the deconvolution of ^{27}Al and ^{29}Si MAS NMR spectra. The ^{29}Si Al MAS-NMR spectra of all Cu-ion-exchanged zeolites

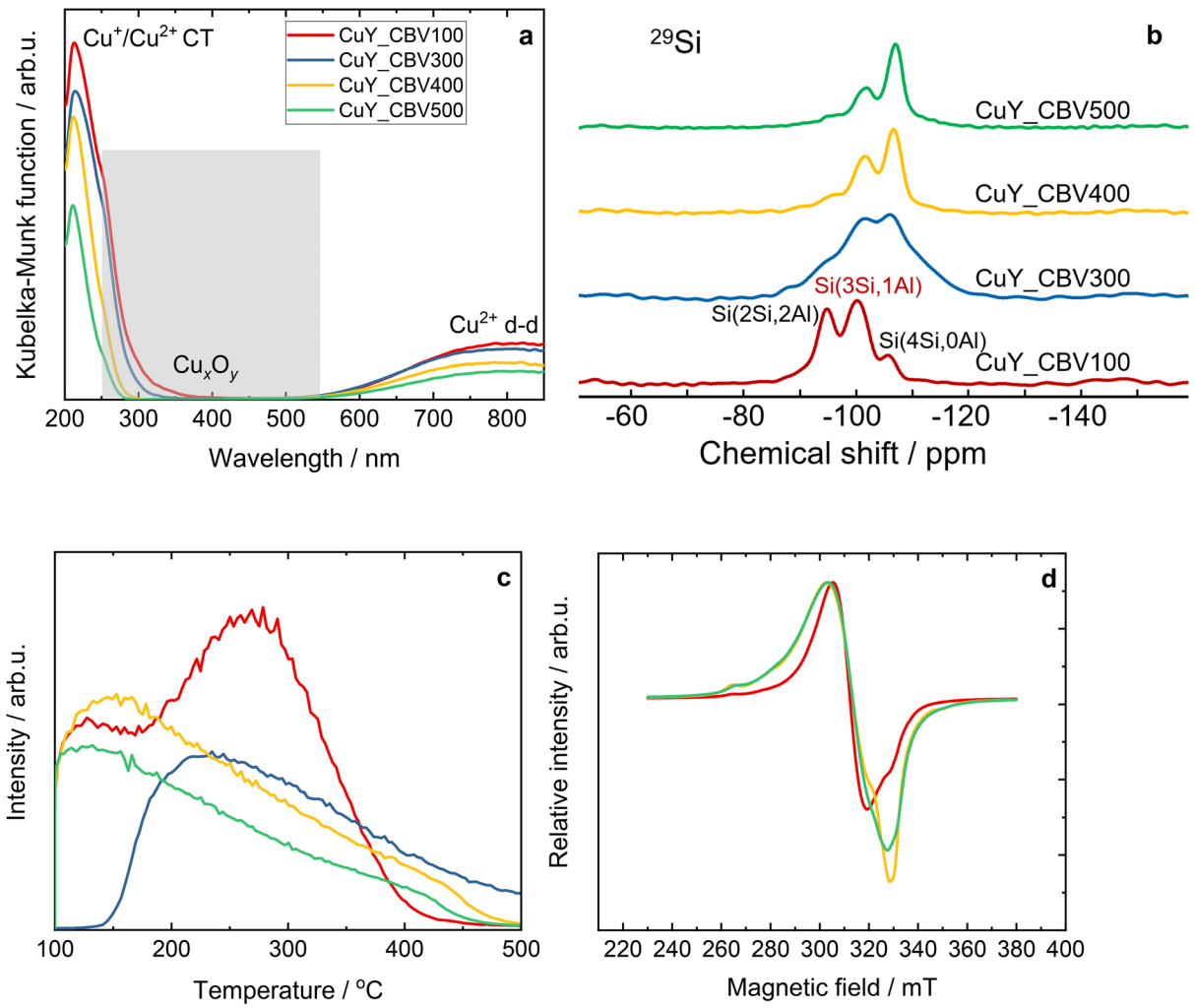

Fig. 2 a) DR UV-vis spectra, b) ^{29}Si MAS spectra and c) NH_3-TPD spectra of Cu-containing zeolite Y samples and d) CW-EPR spectra of the activated samples recorded at −196 °C; a–d) the sample names are the same.

showed that the contribution of Si sites significantly varied among samples. In all spectra, contributions from Si(0Al), Si(1Al), and Si(2Al) are present. In general, an increase of Si(0Al) is observed from CuY_CBV100 to CuY_CBV500. CuY_CBV300 shows broader signals, indicating a large distribution of shifts due to a more disordered arrangement of silicon sites. The ^{27}Al spectra are dominated by the signal at *ca.* 61 ppm, indicating four-coordinated aluminum as expected.[31,32] CuY_CBV100 shows an ordered signal, while the other samples are best described by a distribution of chemical shifts leading to broader signals. Additionally, the amount of five- and especially six-coordinated aluminum increases from CuY_CBV300 to CuY_CBV500. Six-coordinated aluminum is typically assigned to extra-framework aluminum, while five-coordinated aluminum hints at some defects in the structure.

Fig. 2c presents the NH_3-TPD spectra of Cu-containing zeolite Y samples. According to the literature indications, the peak below 200 °C is derived from weakly adsorbed ammonia molecules *via* hydrogen bonding, while the peaks above 200 °C are attributed to strong Brønsted acid sites.[33,34] The tetrahedral framework of these aluminosilicates introduces a negative charge within the zeolite structure. When this charge is balanced by a proton, oxygen becomes bonded to the Si–O–Al bridge, forming hydroxyl groups that serve as strong Brønsted acid sites. The interaction between aluminum and oxygen atoms weakens the O–H bond, thereby enhancing the acidity of the protons in the [–Al–(OH)–Si–] groups.[35] However, as the number of aluminum atoms increases, the framework becomes less unbalanced, resulting in a decrease in the strength of the acid sites. All samples possess a similar n(Si)/n(Al) ratio; however, there are significant differences in Si species. CuY_CBV100 revealed a significant contribution of both Si(2Si, 2Al) and Si(3Si, 1Al), while for other samples, there is an increasing contribution of Si(4Si, 0Al) species. For CuY_CBV100, Na^+ cations are inherently weak Lewis acid sites and contribute to the adsorbed ammonia below 200 °C.

Fig. S6 and 2d show the CW-EPR spectra of the activated samples recorded at −196 °C. The weights of the samples are measured beforehand to get a weight-normalized EPR spectrum for each of the samples afterwards. The samples are measured using X-band continuous wave EPR spectroscopy for the hydrated state (as-made) at −196 °C (Fig. S6). It is evident from the spectrum that the Cu^{2+} species is present in all the samples, and they exhibit different spectral behaviour. Double integration of the EPR spectra indicates the intensity of Cu^{2+} species present in the samples. It is normalized to the Cu^{2+} intensity in CuY_CBV500 and listed in Table S6. After this, all the samples are activated using a vacuum of 1×10^{-2} mbar at a temperature of 250 °C for 2 h and then cooled down gradually back to room temperature. Then, the EPR spectra are recorded to see the changes caused by the activation procedure. Upon simulation using EasySpin 6.0.6,[36] the presence of two species is revealed with an axially symmetric species, species *C* and an isotropic species, species *D*. The spin Hamiltonian parameters used for species *C* are $g_{xx} = g_{yy} = 2.08$ (1), $g_{zz} = 2.33$ (1) and $A_{xx} = A_{yy} = 60$ (8) MHz, $A_{zz} = 520$ (5) MHz; whereas for species *B*, $g_{iso} = 2.16$ (1). The Gaussian line shape is used for both the species, with 2.5 mT broadening for species *C* and 20 mT broadening for species *D*. In this case, nonzero g strain is used and is listed in Table S7. Fig. S7 shows the weighted average experimental spectra and the simulated spectra for all the activated samples. The species *C* arises from the Cu^{2+} ions present in the hexagonal prism of the zeolite, bound to six zeolitic oxygens.[37] The species *D* arises from a high local concentration of Cu^{2+} that could potentially be from the higher local concentration of species *C*.[37] The weight of the individual species is given in Table S8 (uncertainty 5%). Based on this analysis, we have isolated magnetically diluted Cu^{2+} species as hexaaqua water complexes exist in the fresh material and as Cu^{2+} in the hexagonal prisms bound to six framework oxygens. But the majority of the Cu^{2+} appears as non-magnetically diluted Cu^{2+}, in either hexaaquawater complexes or presumably also hexagonal prisms. The amount of thelatter seems to increase after activation, especially in the CuY_CBV100 sample. Indeed, Cu^{2+} species serve as active centers for low temperature during NH_3-SCR-DeNO$_x$.[21]

3.2. Catalytic studies and sample-specific insights into NH_3-SCR-DeNO$_x$

Fig. 3 shows the NO conversion and selectivity of Cu-containing zeolites during NH_3-SCR-DeNO$_x$. Similar to our previous studies,[21] CuY_CBV100 approved the highest activity together with the highest formation of N_2O. Similarly, CuY_CBV500 shows NO conversion below 80% below 300 °C, with N_2 selectivity above 85%. Interestingly, we did not observe any differences in the catalytic data for the samples prepared from as-received zeolites compared to calcined zeolites (before ion exchange with a copper precursor).

Both CuY_CBV300 and CuY_CBV400 possess similar activity and N_2 selectivity in NH_3-SCR-DeNO$_x$, as in fact it is the same support zeolite Y (starting form of CBV300 is in NH_4^+, while for CBV400 it is H^+). Dynamic changes of Cu-containing zeolite Y samples (Fig. S8) were investigated in six consecutive reactions of heating up (75–500 °C) and cooling down (500–75 °C). The catalysts revealed stable NO conversion and N_2 selectivity.

Furthermore, we conducted stop flow studies for all catalysts at 125 °C (Fig. 3c and d and S9). Thus, NH_3-SCR-DeNO$_x$ was conducted at 125 °C for 2 h, followed by purging in He for 3 h and finally, temperature-programmed studies from 125 °C up to 500 °C. In addition to NH_3 (mass-to-charge ratio (m/z) 17) and/or NO (m/z 30) desorption, the detection of reaction products such as N_2 (m/z 28), N_2O (m/z 44), NO_2 (m/z 46), and H_2O (m/z 18) was also conducted. The stop flow analysis revealed that the adsorbed ammonia was the main difference between CuY_CBV100 and CuY_CBV300 (300 500), and thus, their

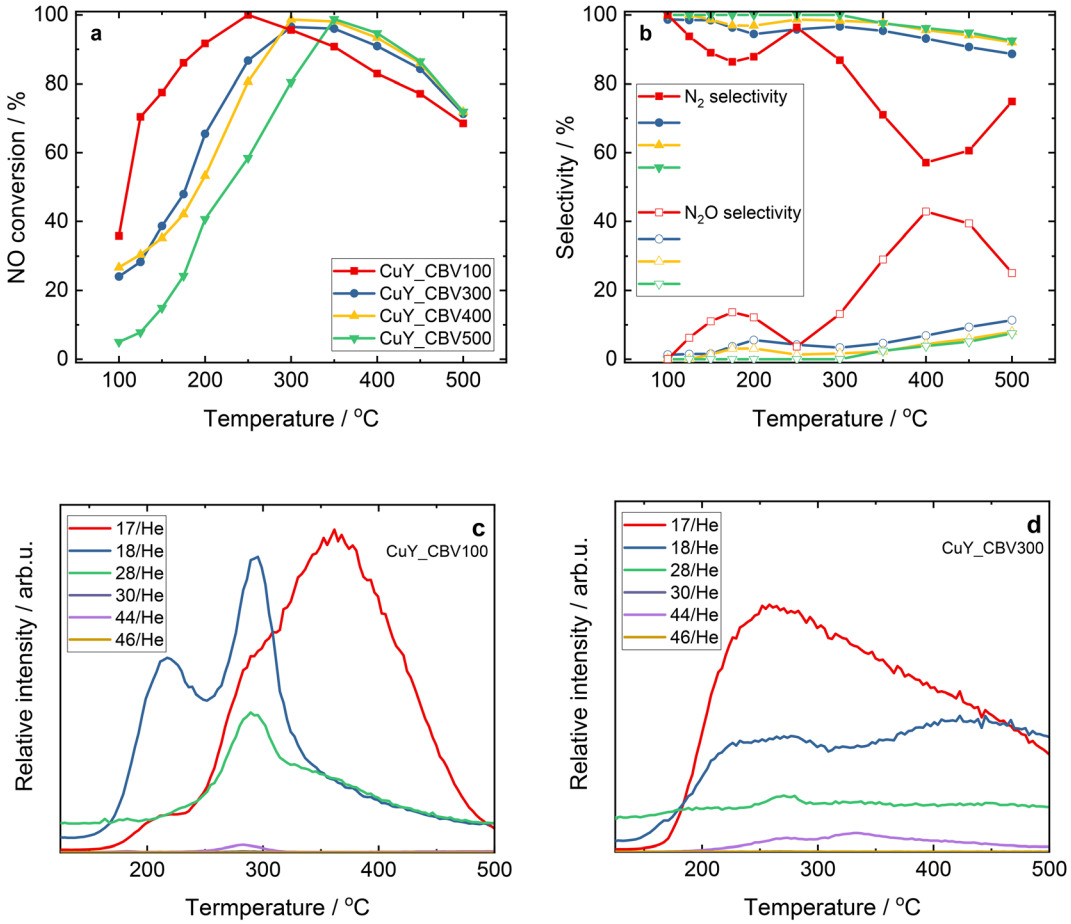

Fig. 3 a) NO conversion and b) N_2 and N_2O selectivity during NH_3-SCR-DeNO$_x$ over Cu-containing Y samples; a) and b) the sample names are the same. c) and d) Stop-flow experiments over Cu-containing Y samples. Reaction conditions: m_K = 0.1 g, c(NO) = 0.1 vol%, c(NH_3) = 0.1 vol%, c(O_2) = 5 vol%, He balance, F_{TOT} = 120 ml min^{-1}, GHSV = 30 000 h^{-1}.

accessibility for NO molecules from the gas phase during the NH_3-SCR-DeNO$_x$ and NH_3 oxidation above 350 °C. Also, the shape of the NH_3 adsorbed during stop-flow analysis is similar to the one detected during NH_3-TPD profiles (Fig. 3c and d *vs.* 2c). Additionally, we carried out modulation excitation diffuse reflectance infrared Fourier transform spectroscopy (ME DRIFTS). From Fig. 4a, only NH_3 adsorbed on Lewis acid sites (L-NH_3) is observed on CuY_CBV100. When the NH_3 adsorbed surface of CuY_CBV100 is exposed to NO, the L-NH_3 decreases, and a peak at *ca.* 1440 cm^{-1} and a band between 3000 and 2000 cm^{-1} rise. It indicates that L-NH_3 is consumed by NO, and the H_2O product is formed, which does not leave the surface and adsorbs to induce these peaks due to the relatively low temperature. One possibility that cannot be ruled out is that the H_2O product induces the formation of Brønsted acid sites,[38,39] then some L-NH_3 moves to the BAS and induces the peaks of 1440 cm^{-1}. For CuY_CBV300, CuY_CBV400, and CuY_CBV500, L-NH_3 and B-NH_3 are detected, and the amount of B-NH_3 is ranked as CuY_CBV300 < CuY_CBV400 < CuY_CBV500. This means that there are more BAS on CuY_CBV500. When the NH_3 adsorbed surface of CuY_CBV500 is exposed to NO, L-NH_3 and B-NH_3 both decrease, which means that they are consumed by NO.

For CuY_CBV100, peaks at 1650, 1614 and 1440 cm^{-1} show an obvious response to the NO pulse in NH_3 + O_2, and the peak at 1614 shows opposite dynamic change compared to the peak at 1650 cm^{-1}, similar to that at 1440 cm^{-1}. This means that the consumption of L-NH_3 induces the formation of species attributed to 1650 and 1440 cm^{-1}. Furthermore, the peak at 1440 cm^{-1} shows a slight delay compared to 1650 cm^{-1}, which might be due to the reason that the species at 1650 cm^{-1} induces the formation of species at 1440 cm^{-1}. For CuY_CBV300, CuY_CBV400, and CuY_CBV500, the intensity of response to the NO pulse is obviously lower than that of CuY_CBV100, and they are ranked as CuY_CBV300 > CuY_CBV400 > CuY_CBV500.

In addition, the peak at 1620 cm^{-1} shows opposite dynamic change compared to the peak at 1450 cm^{-1}. It seems that LAS domains trigger this reaction (Fig. 5 and S10).

Recently, Kubota *et al.*[9] published molecular aspects of the mechanism of NH_3-SCR-DeNO$_x$ on tungsten-loaded ceria from modulated excitation DRIFTS. This mechanism seems

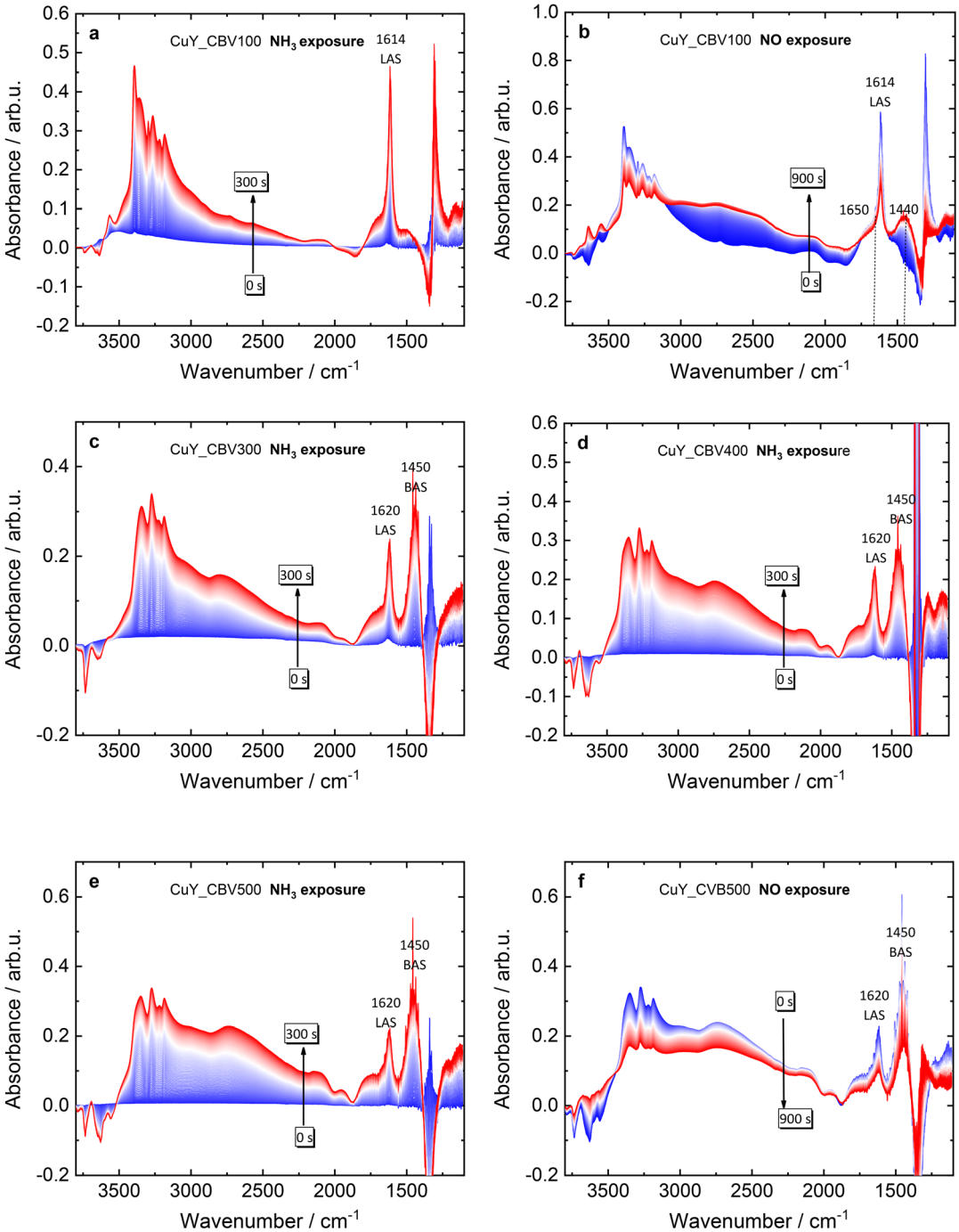

Fig. 4 Time-resolved *in situ* IR spectra of NH_3 adsorption (a) and NO exposure (b) on CuY_CBV100, time-resolved *in situ* IR spectra of NH_3 adsorption on CuY_CBV300 (c) and CuY_CBV400 (d), and time-resolved *in situ* IR spectra of NH_3 adsorption (e) and NO exposure (f) on CuY_CBV500.

to be valid also, in our case. Thus, we could assume that during the NH_3-SCR-DeNO$_x$ process, NH_3 adsorbed on Cu^{2+} Lewis acid sites reacts with NO to produce Cu^+ sites, N_2, H_2O, and H^+ associated with Brønsted acid sites. The protons from the initially adsorbed Lewis acid sites desorbs and are subsequently re-adsorbed onto the newly formed Brønsted acid sites, while Cu^{2+} is regenerated through oxidation facilitated by O_2 and H^+.

Fig. 6 presents the results of the SSITKA analysis between 100 and 150 °C for the Cu-containing zeolite Y. Under steady-state conditions, switching between unlabeled and labeled reaction mixtures was performed without perturbation. Consequently, the total rate of formation of any product (*i.e.*, the chemical composition of the surface) does not change due to the abrupt replacement of one reactant by its isotope. In this way, kinetic parameters such as the average surface

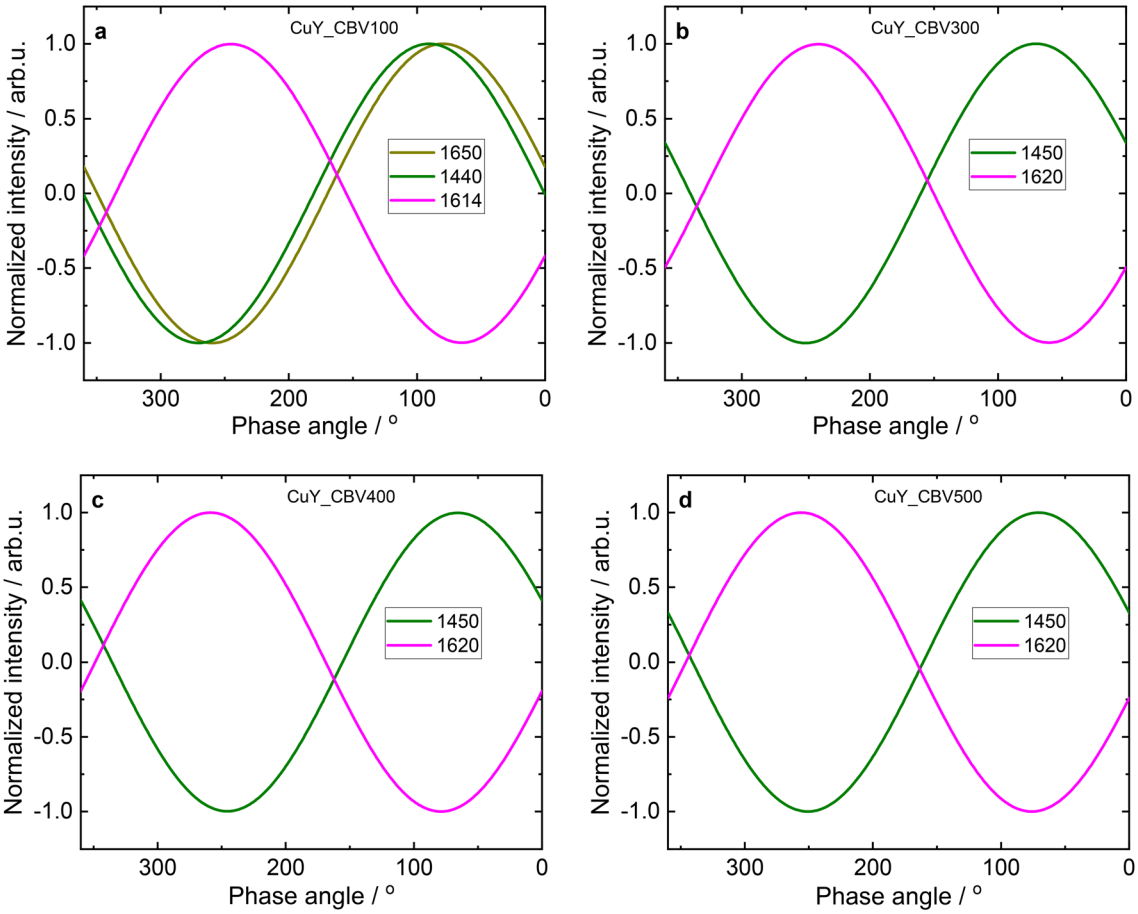

Fig. 5 Phase angle dependence of the IR signal intensity of selected peaks on CuY_CBV100 (a) and CuY_CBV300 (b) and the phase angle dependence of the IR signal intensity of selected peaks on CuY_CBV400 (c) and CuY_CBV500 (d).

lifetime and surface concentration of the main intermediates (not of any inactive (spectator) species) can be determined. The SSITKA studies were carried out at 100, 125, and 150 °C. Compared to our previous work,[21] we applied two measurement times: 5 and 10 minutes in order to check how the rates of change in these kinetic parameters differ among the studied catalysts. For all materials, the average surface lifetime of reversibly adsorbed NH_3 increased with time; however, it did not change significantly with the applied temperature. On the other hand, the surface concentration of reversibly adsorbed NH_3 decreases with increasing temperature, suggesting that the concentration of inactive NH_3 molecules on the catalyst surface decreases. These changes agreed with the catalytic activity results (Fig. 3a) – the most active catalyst (CuY_CBV100) adsorbs the lowest amounts of inactive NH_3 molecules, while the least active catalyst (CuY_CBV500) adsorbs the highest quantities of inactive amonium molecules. In the case of CuY_CBV300 and CuY_CBV400, the values of the surface concentration of reversibly adsorbed NH_3 are very similar to each other, because their activity is also very similar.

Based on the SSITKA results, the average surface lifetime and surface concentration of nitrogen and its intermediates involved in nitrogen formation were also calculated (Fig. 6b, d, f and h). The average surface lifetime values for the analysed temperatures (100, 125, and 150 °C) are very similar, whereas some slight differences are observed between the studied catalysts. The most interesting behaviour is observed for the values of the surface concentration of nitrogen and its intermediates involved in nitrogen formation. Extending the analysis time to 10 min allowed for obtaining higher values of the average-surface lifetime and surface concentrations, but did not vary the trend of their changes with temperature.

The highest values were obtained for CuY_CBV100, which is the most active catalyst. This means that, on its surface, there are the most considerable amounts of active centres. In the case of CuY_CBV300 and CuY_CBV400, these values are similar but lower than those for CuY_CBV100. These two catalytic materials (CuY_CBV300 and CuY_CBV400) exhibit practically the same, but lower, activity in the NH_3-SCR-$DeNO_x$ process. The worst catalytic material (CuY_CBV500 catalyst) shows the lowest (below 20 mmol g^{-1}) surface concentration of nitrogen and its intermediates involved in nitrogen formation in all the studied measurements.

To summarize this part, it can be stated that although all catalytic materials adsorb large amounts of ammonia (Fig. 2c), only a part of these sites becomes active for the

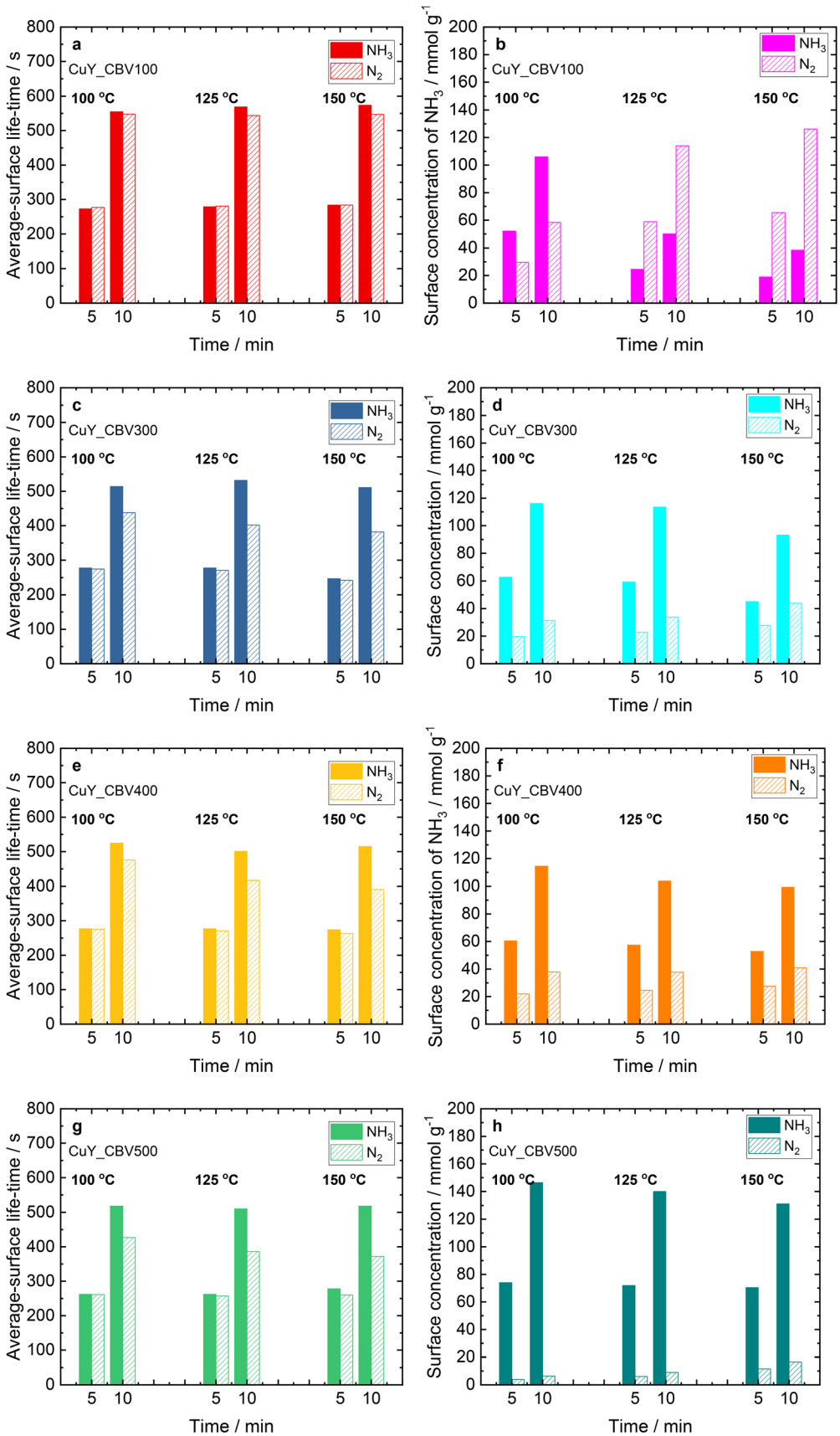

Fig. 6 a, c, e and g) Average-surface lifetime of reversibly adsorbed ammonia, adsorbed nitrogen molecules, and intermediates leading to the formation of nitrogen and b, d, f and h) surface concentration of reversibly adsorbed ammonia, adsorbed nitrogen molecules, and intermediates leading to the formation of nitrogen.

NH_3-SCR-DeNO$_x$ process. This behavior is correlated with the increase in acidity (*i.e.*, Lewis acid sites) of the catalytic materials.

4. Conclusions

A series of copper-modified commercial zeolite Y catalysts were investigated for their activity and N_2 selectivity in the NH_3-SCR-DeNO$_x$ reaction. Modulated excitation *in situ*/operando infrared (IR) spectroscopy and phase-sensitive detection (PSD) were applied to study the reaction intermediates that formed on the Cu-containing Y zeolite samples during transient experiments. For CuY_CBV100, after NO exposure to the NH_3 preadsorbed surface, the NH_3 adsorbed on Lewis acid sites (L-NH_3) decreases, while new Brønsted acid sites form (B-NH_3). Then, some L-NH_3 moves to the BAS. Thus, the LAS domains govern the NH_3-SCR-DeNO$_x$ reaction. For modulation excitation results, for CuY_CBV300, CuY_CBV400, and CuY_CBV500, the intensity of the response to the NO pulse is obviously lower than that of CuY_CBV100. As for CuY_CBV500, the situation is different; we can see that the B-NH_3 peak is quite strong, which means a large number of BAS exist on the CuY_CBV500 surface. NO can react with both L-NH_3 and B-NH_3 (whose presence facilitates high N_2 selectivity).

By the application of SSITKA, we determined the average-surface lifetime and surface concentration of NH_3, nitrogen and intermediates leading to the formation of nitrogen at different temperatures and times of exchange of NH_3. The number of active sites was found as the key parameter for the activity of CuY_CBV100 in NH_3-SCR-DeNO$_x$, while N_2 selectivity is determined by slower rates of ammonia consumption during the reaction, as for CuY_CBV500.

Author contributions

Magdalena Jabłońska: conceptualization, methodology, investigation, data curation, writing – original draft and review & editing, supervision, data management, project management, and resources. Rujito S. R. Suharbiansah: investigation, data curation, and writing – review & editing. Jie Yang: investigation, data curation, and writing – review & editing. Marek Rotko: data curation and review. Pranjit Das: investigation, data curation, and writing – review & editing. Marko Bertmer: investigation and data curation. Jacek Grams: investigation and data curation. Junjiang Zhu: review. Andreas Pöppl: review.

Conflicts of interest

There are no conflicts to declare.

Data availability

The data supporting this article have been included as part of the supplementary information (SI).

Supplementary information is available. See DOI: https://doi.org/10.1039/d5cy01536g.

Acknowledgements

M. J. and M. R. acknowledge NAWA-DAAD Nr.BPN/BDE/2023/1/00001/U/00001.

References

1 M. Jabłońska, M. E. Potter and A. M. Beale, Recent Progress in the Application of transition-metal containing MFI topologies for NH_3-SCR-DeNO$_x$ and NH_3 oxidation, *ChemCatChem*, 2024, **16**, e202301214.
2 G. Dai, B. Liu, R. Wang, H. Wang, Y. Miao, S. Hou, D. Lian, M. Chen, C. Li, Z. Zhang and others, Pretreatment techniques in CO-SCR and NH_3-SCR: Status, challenges, and perspectives, *J. Catal.*, 2024, 115925.
3 T. Seiyama, T. Arakawa, T. Matsuda, Y. Takita and N. Yamazoe, Catalytic activity of transition metal ion exchanged Y zeolites in the reduction of nitric oxide with ammonia, *J. Catal.*, 1977, **48**, 1–7.
4 F. Gramigni, N. D. Nasello, N. Usberti, U. Iacobone, T. Selleri, W. Hu, S. Liu, X. Gao, I. Nova and E. Tronconi, Transient kinetic analysis of low-temperature NH_3-SCR over Cu-CHA catalysts reveals a quadratic dependence of Cu reduction rates on Cu^{II}, *ACS Catal.*, 2021, **11**, 4821–4831.
5 N. Usberti, F. Gramigni, N. D. Nasello, U. Iacobone, T. Selleri, W. Hu, S. Liu, X. Gao, I. Nova and E. Tronconi, An experimental and modelling study of the reactivity of adsorbed NH_3 in the low temperature NH_3-SCR reduction half-cycle over a Cu-CHA catalyst, *Appl. Catal., B*, 2020, **279**, 119397.
6 K. A. Tarach, M. Jabłońska, K. Pyra, M. Liebau, B. Reiprich, R. Gläser and K. Góra-Marek, Effect of zeolite topology on NH_3-SCR activity and stability of Cu-exchanged zeolites, *Appl. Catal., B*, 2021, **284**, 119752.
7 A. M. Robles, M. Jabłońska, A. Palčić, M. Bubaš, J. Yang, M. Rotko, M. F. Lukman, A. Guo, M. Bertmer, M. Huš and others, Cu-SSZ-13 catalysts designed through interzeolite conversion process from different structure types of zeolites for NH_3-SCR-DeNO$_x$: Structure-property activity relationships and intermediates determination, *ChemCatChem*, 2025, **17**, e01017.
8 A. Oda, H. Shionoya, Y. Hotta, T. Takewaki, K. Sawabe and A. Satsuma, Spectroscopic evidence of efficient generation of dicopper intermediate in selective catalytic reduction of NO over Cu-ion-exchanged zeolites, *ACS Catal.*, 2020, **10**, 12333–12339.
9 H. Kubota, Y. Qian, S. Mine, T. Toyao, R. J. G. Nuguid, F. Buttignol, D. Ferri and K. Shimizu, Molecular aspects of the mechanism of NH_3-SCR on tungsten-loaded ceria from modulated excitation DRIFTS, *ChemCatChem*, 2025, **17**, e202401839.
10 A. Urakawa, T. Bürgi and A. Baiker, Sensitivity enhancement and dynamic behavior analysis by modulation excitation

spectroscopy: Principle and application in heterogeneous catalysis, *Chem. Eng. Sci.*, 2008, **63**, 4902–4909.
11 D. Ferri, M. A. Newton and M. Nachtegaal, Modulation excitation X-ray absorption spectroscopy to probe surface species on heterogeneous catalysts, *Top. Catal.*, 2011, **54**, 1070.
12 P. Müller and I. Hermans, Applications of modulation excitation spectroscopy in heterogeneous catalysis, *Ind. Eng. Chem. Res.*, 2017, **56**, 1123–1136.
13 R. J. G. Nuguid, D. Ferri, A. Marberger, M. Nachtegaal and O. Kröcher, Modulated excitation Raman spectroscopy of V_2O_5/TiO_2: mechanistic insights into the selective catalytic reduction of NO with NH_3, *ACS Catal.*, 2019, **9**, 6814–6820.
14 R. J. G. Nuguid, M. Elsener, D. Ferri and O. Kröcher, Operando diffuse reflectance infrared detection of cyanide intermediate species during the reaction of formaldehyde with ammonia over V_2O_5/WO_3-TiO_2, *Appl. Catal., B*, 2021, **298**, 120629.
15 A. Marberger, A. W. Petrov, P. Steiger, M. Elsener, O. Kröcher, M. Nachtegaal and D. Ferri, Time-resolved copper speciation during selective catalytic reduction of NO on Cu-SSZ-13, *Nat. Catal.*, 2018, **1**, 221–227.
16 P. Biloen, Transient kinetic methods, *J. Mol. Catal.*, 1983, **21**, 17–24.
17 C. O. Bennett, in *ACS Symposium Series*, ed. A. T. Bell and L. L. Hegedus, American Chemical Society, Washington, DC, 1982, vol. 178, p. 1.
18 J. Happel, Transient tracing, *Chem. Eng. Sci.*, 1978, **33**, 1567.
19 P. Winslow and A. T. Bell, Application of transient response techniques for quantitative determination of adsorbed carbon monoxide and carbon present on the surface of a ruthenium catalyst during Fischer-Tropsch synthesis, *J. Catal.*, 1984, **86**, 158–172.
20 M. Jabłońska, An Application of Steady-state isotopic-transient kinetic analysis (SSITKA) in $DeNO_x$ process, *ChemCatChem*, 2021, **13**, 818–827.
21 M. Jabłońska, R. S. R. Suharbiansah, K. Góra-Marek, M. Rotko, M. Ruszak, M. Fernadi Lukman, A. Palcic, R. Denecke, M. Bertmer, J. Grams and others, NH_3-SCR-$DeNO_x$ activity of Cu-containing commercial zeolite Y, *Ind. Eng. Chem. Res.*, 2024, **63**, 17075–17085.
22 M. Jabłońska, A. Mollá Robles, M. Rotko, T. H. Vuong, H. Lei, Ž. Lavrič, M. Grilc, M. F. Lukman, R. Valiullin, M. Bertmer, J. Möllmer, J. Rabeah, A. Pöppl, U. Simon and R. Gläser, Unraveling the NH_3-SCR-$DeNO_x$ mechanism of Cu-SSZ-13 variants by spectroscopic and transient techniques, *ChemSusChem*, 2024, **17**, e202400198.
23 https://www.zeolyst.com/our-products/standard-zeolite-powders/zeolite-y.html.
24 D. Verboekend, N. Nuttens, R. Locus, J. Van Aelst, P. Verolme, J. C. Groen, J. Pérez-Ramírez and B. F. Sels, Synthesis, characterisation, and catalytic evaluation of hierarchical faujasite zeolites: milestones, challenges, and future directions, *Chem. Soc. Rev.*, 2016, **45**, 3331–3352.
25 M. Thommes, K. Kaneko, A. V. Neimark, J. P. Olivier, F. Rodriguez-Reinoso, J. Rouquerol and K. S. W. Sing, Physisorption of gases, with special reference to the evaluation of surface area and pore size distribution (IUPAC Technical Report), *Pure Appl. Chem.*, 2015, **87**, 1051–1069.
26 R. S. R. Suharbiansah, M. F. Lukman, C. Nannuzzi, A. Wach, K. Góra-Marek, M. Liebau, A. Palčić, A. Pöppl, G. Berlier and S. Bordiga, Effect of the preparation method on the catalytic properties of copper-containing zeolite Y applied for NH_3-SCR-$DeNO_x$, *Catal. Sci. Technol.*, 2023, **13**, 3804–3817.
27 Q. Huo, D. I. Margolese and G. D. Stucky, Surfactant control of phases in the synthesis of mesoporous silica-based materials, *Chem. Mater.*, 1996, **8**, 1147–1160.
28 L. Martins, R. P. S. Peguin, M. Wallau and others, Cu-, Co-, Cu/Ca-and Co/Ca-exchanged ZSM-5 zeolites: Activity in the reduction of NO with methane or propane, in *Stud. Surf. Sci. Catal.*, Elsevier, 2004, pp. 2475–2483.
29 M. Jabłońska, K. Góra-Marek, M. Grilc, P. C. Bruzzese, D. Poppitz, K. Pyra, M. Liebau, A. Pöppl, B. Likozar and R. Gläser, Effect of textural properties and presence of co-cation on NH_3-SCR activity of Cu-exchanged ZSM-5, *Catalysts*, 2021, **11**, 843.
30 A. Palčić, P. C. Bruzzese, K. Pyra, M. Bertmer, K. Góra-Marek, D. Poppitz, A. Pöppl, R. Gläser and M. Jabłońska, Nanosized Cu-SSZ-13 and its application in NH_3-SCR, *Catalysts*, 2020, **10**, 1–21.
31 G. J. Ray, B. L. Meyers and C. L. Marshall, 29Si and 27Al nmr study of steamed faujasites-Evidence for non-framework tetrahedrally bound aluminium, *Zeolites*, 1987, **7**, 307–310.
32 B. Xu, S. Bordiga, R. Prins and J. A. van Bokhoven, Effect of framework Si/Al ratio and extra-framework aluminum on the catalytic activity of Y zeolite, *Appl. Catal., A*, 2007, **333**, 245–253.
33 J. V. Milato, R. J. França and M. R. C. Marques, Pyrolysis of oil sludge from the offshore petroleum industry: influence of different mesoporous zeolites catalysts to obtain paraffinic products, *Environ. Technol.*, 2021, **42**, 1013–1022.
34 J. Van Aelst, D. Verboekend, A. Philippaerts, N. Nuttens, M. Kurttepeli, E. Gobechiya, M. Haouas, S. P. Sree, J. F. M. Denayer, J. A. Martens and others, Catalyst design by NH4OH treatment of USY zeolite, *Adv. Funct. Mater.*, 2015, **25**, 7130–7144.
35 B. M. Weckhuysen and J. Yu, Recent advances in zeolite chemistry and catalysis, *Chem. Soc. Rev.*, 2015, **44**, 7022–7024.
36 S. Stoll and A. Schweiger, EasySpin, a comprehensive software package for spectral simulation and analysis in EPR, *J. Magn. Reson.*, 2006, **178**, 42–55.
37 J. S. Yu and L. Kevan, Temperature dependence of copper (II) migration and formation of new copper (II) species during catalytic propylene oxidation on copper (II)-exchanged Y zeolite and comparison with X zeolite, *J. Phys. Chem.*, 1990, **94**, 7612–7620.
38 R. J. G. Nuguid, L. Ortino-Ghini, V. L. Suskevich, J. Yang, L. Lietti, O. Kröcher and D. Ferri, Interconversion between Lewis and Brønsted-Lowry acid sites on vanadia-based catalysts, *Phys. Chem. Chem. Phys.*, 2022, **24**, 4555–4561.
39 I. Song, H. Lee, S. W. Jeon and D. H. Kim, Understanding the dynamic behavior of acid sites on TiO_2-supported vanadia catalysts via operando DRIFTS under SCR-relevant conditions, *J. Catal.*, 2020, **382**, 269–279.